Supporting information

Hydrogen-bonded organic framework-derived, flower-on-fiber-like, carbon nanofiber electrode for supercapacitors

Woo Jin Mun, Bomi Kim, Seung Jae Moon and Jong Hak Kim*

Department of Chemical and Biomolecular Engineering, Yonsei University, 50 Yonsei-ro, Seodaemun-gu, Seoul 03722, South Korea

* To whom correspondence should be addressed

Tel: +82-2-2123-5757; Fax: +82-2-312-6401

E-mail: jonghak@yonsei.ac.kr

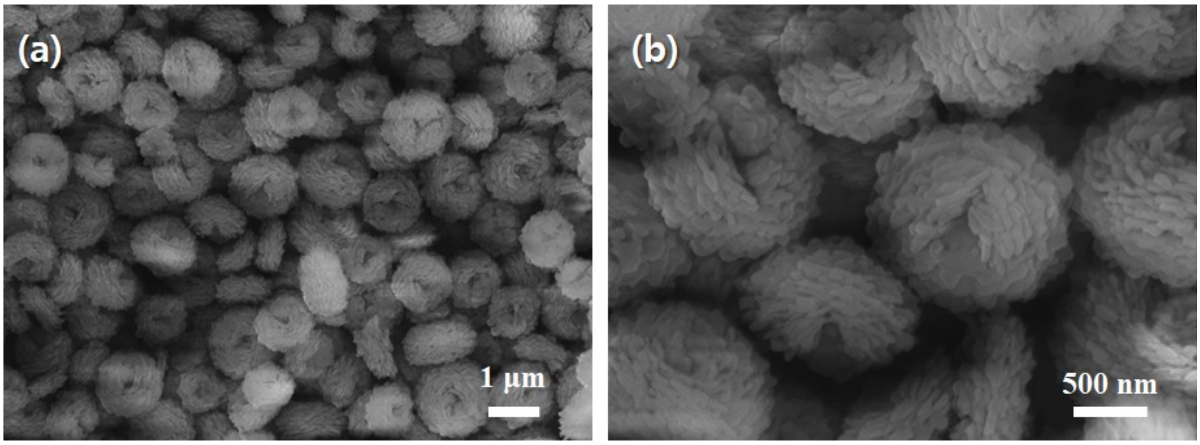

Fig. S1. (a, b) SEM images of MCA.

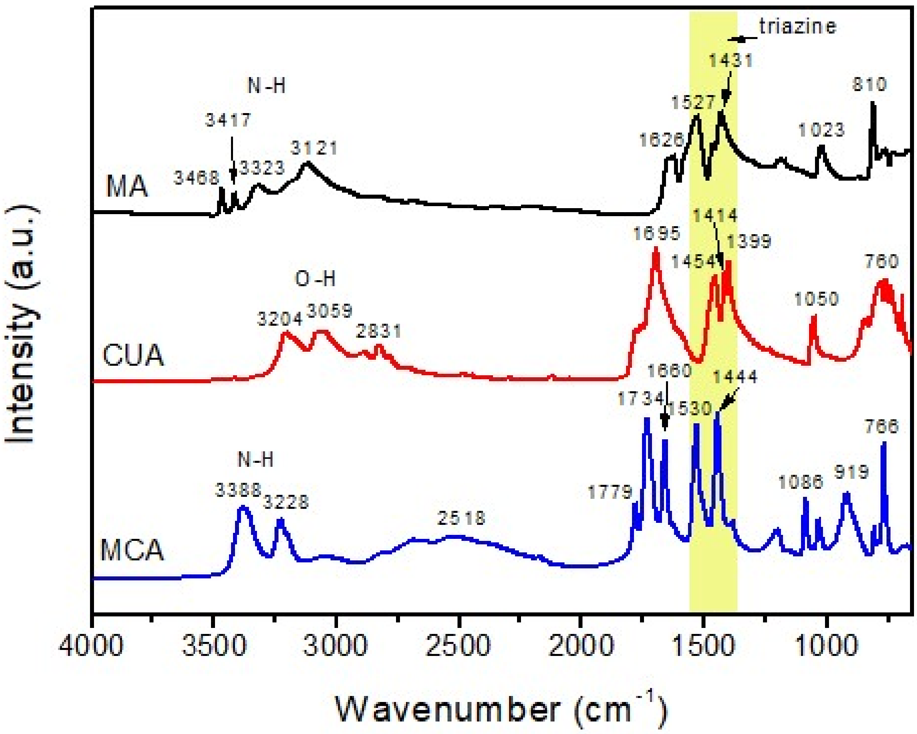

Fig. S2. FT-IR spectra of MA, CUA, and MCA.

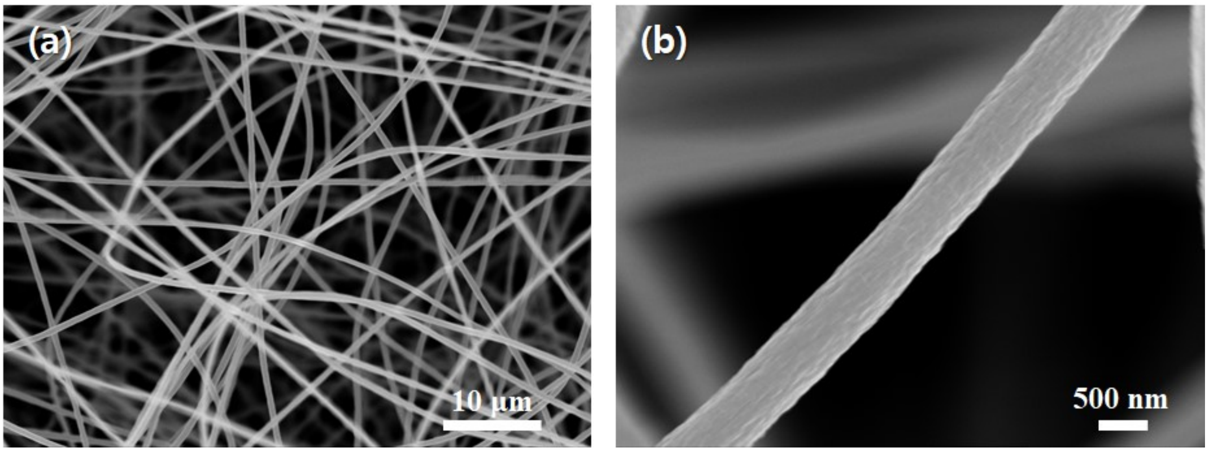

Fig S3. (a, b) SEM images of PAN nanofibers.

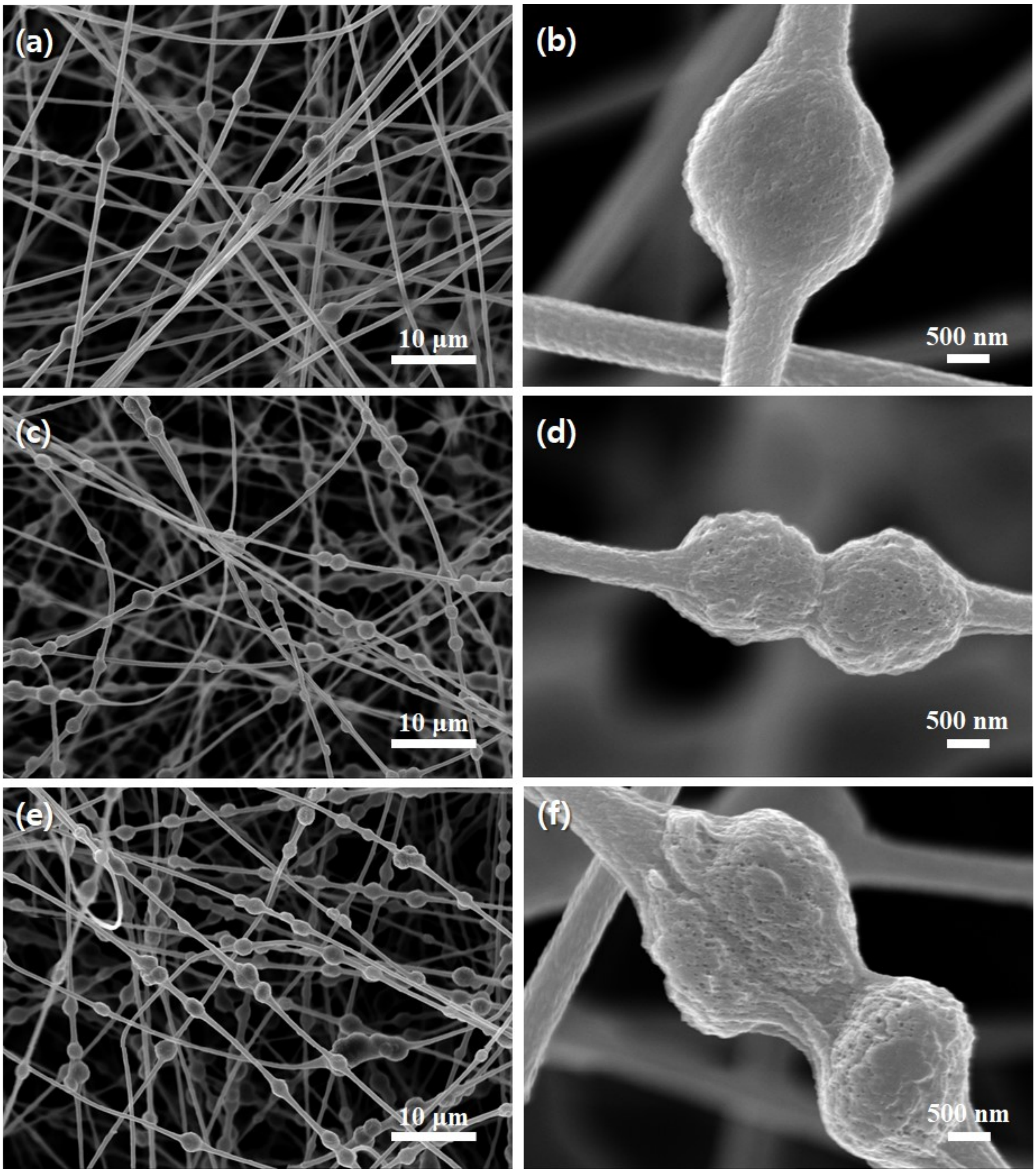

Fig. S4. SEM images of (a, b) PAN@$MCA_{0.125}$, (c, d) PAN@$MCA_{0.375}$, and (e, f) PAN@$MCA_{0.5}$ nanofibers.

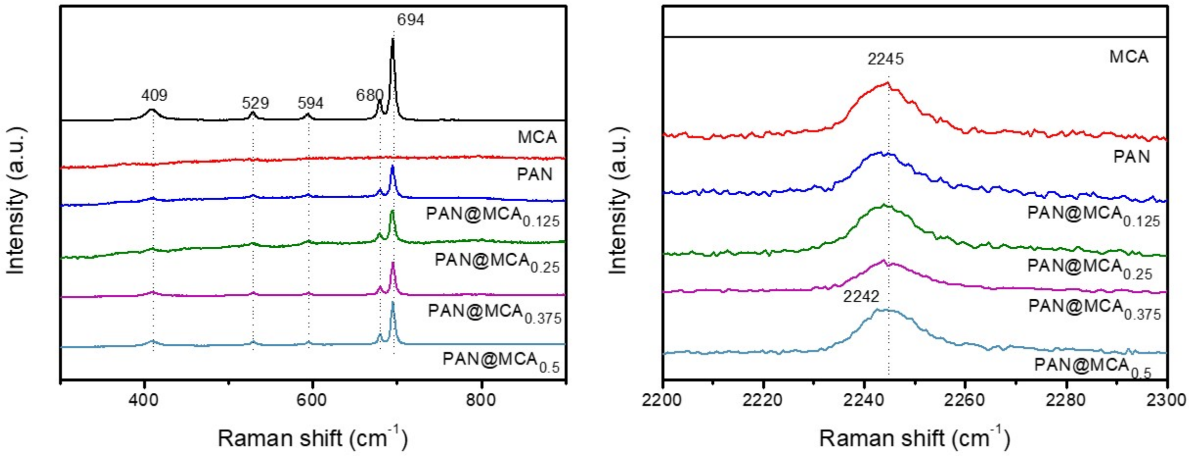

Fig. S5. (a, b) Raman spectra of MCA, PAN, and PAN@MCA nanofibers.

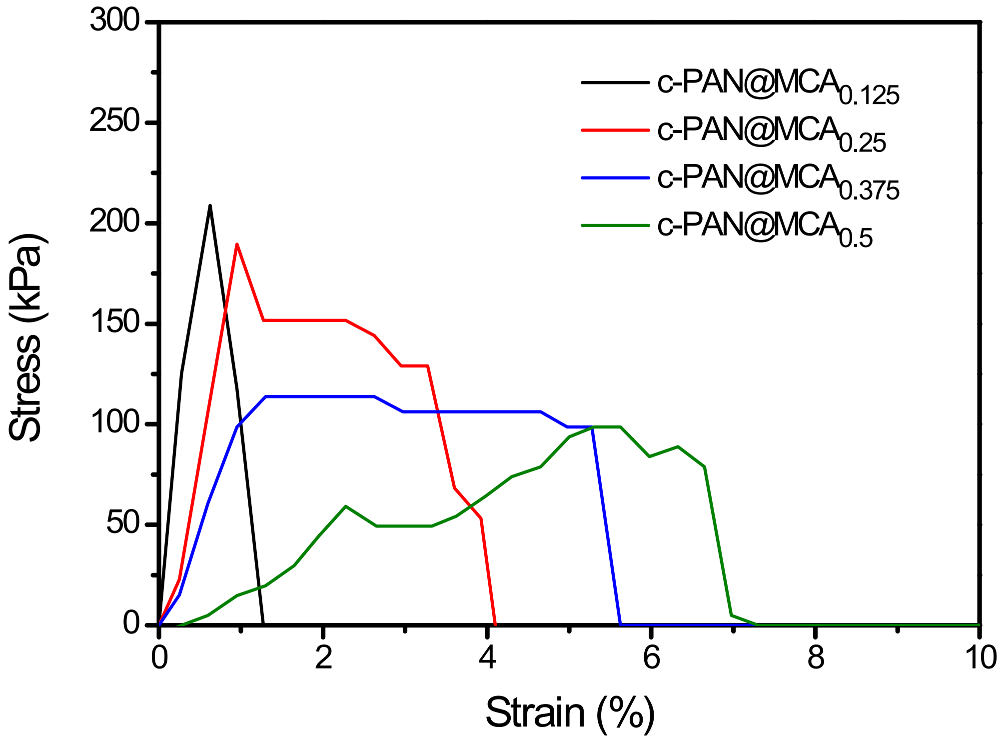

Fig. S6. Stress-strain curves of c-PAN@MCA nanofibers.

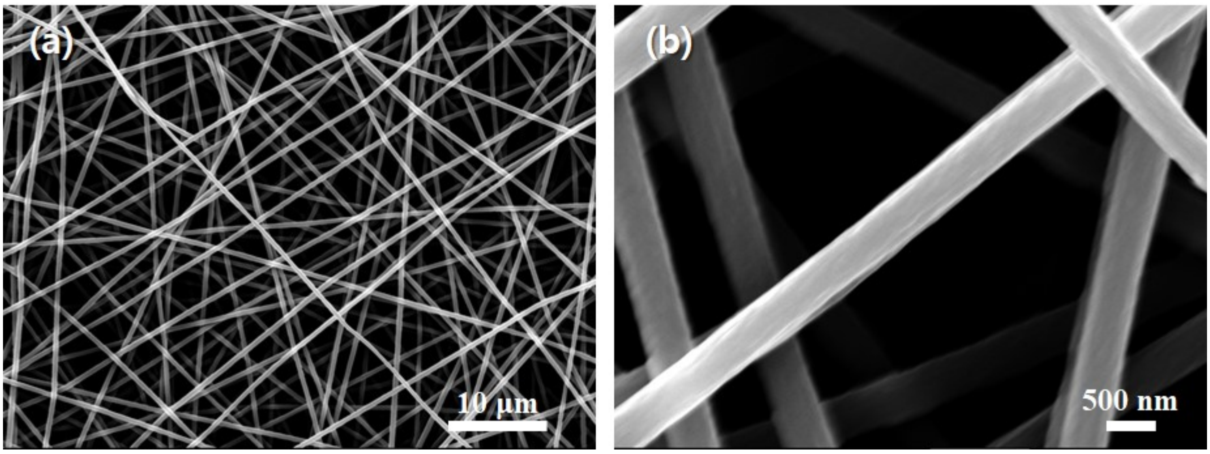

Fig. S7. (a, b) SEM images of c-PAN nanofibers.

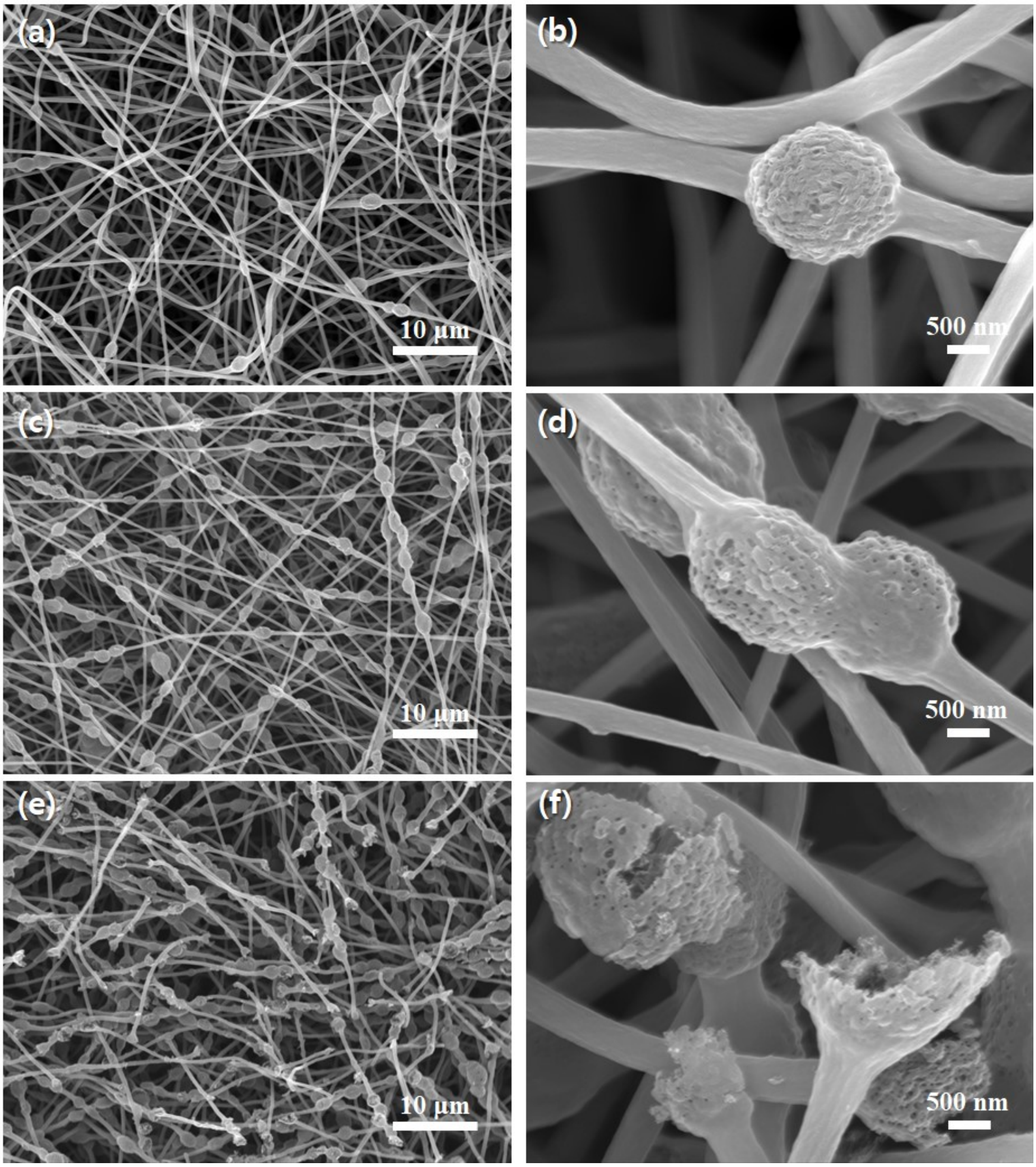

Fig. S8. SEM images of (a, b) c-PAN@$MCA_{0.125,}$ (c, d) c-PAN@$MCA_{0.375}$, and (e, f) c-PAN@$MCA_{0.5}$ nanofibers.

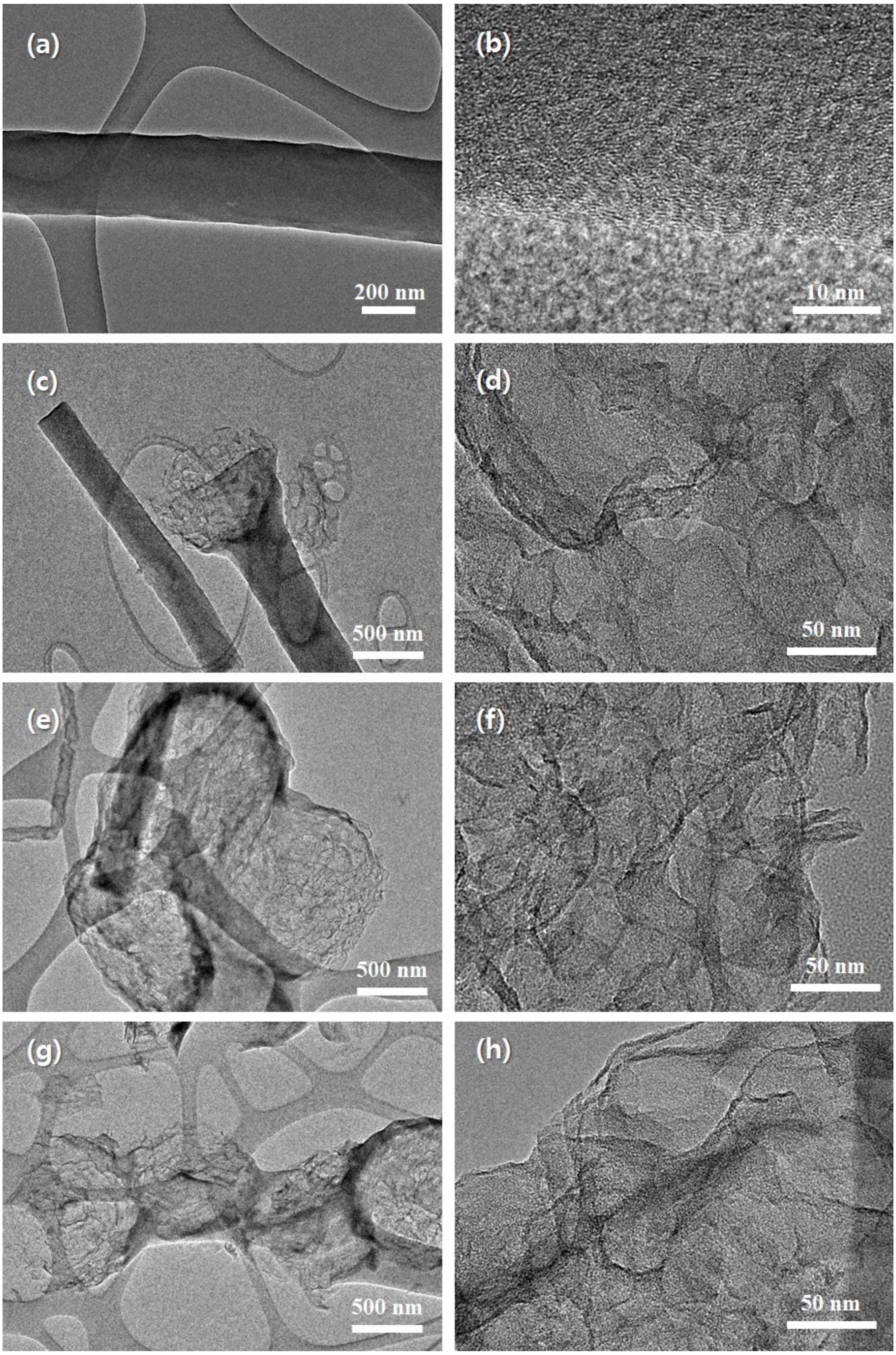

Fig. S9. TEM images of (a, b) c-PAN, (c, d) c-PAN@$MCA_{0.125}$, (e, f) c-PAN@$MCA_{0.375}$, and (g, h) c-PAN@$MCA_{0.5}$ nanofibers.

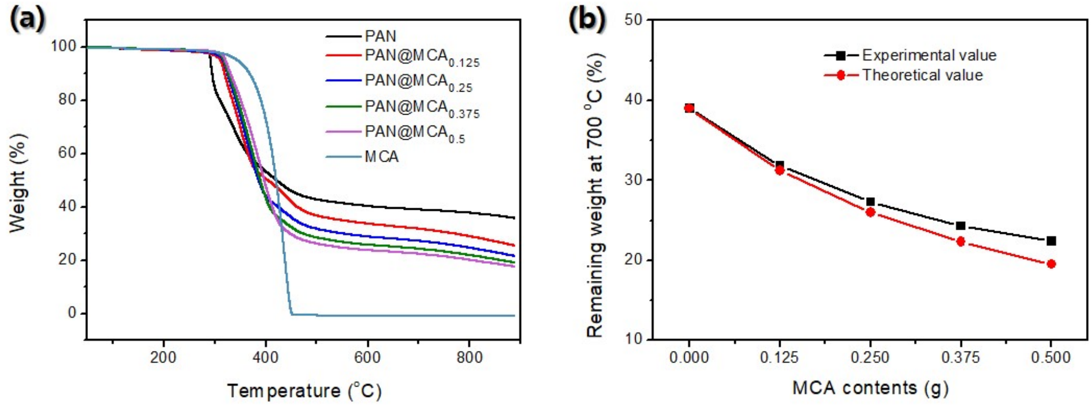

Fig. S10. (a) TGA curves of PAN, PAN@MCA nanofibers, and MCA. (b) Experimental and theoretical remaining weight at 700 °C with various MCA contents.

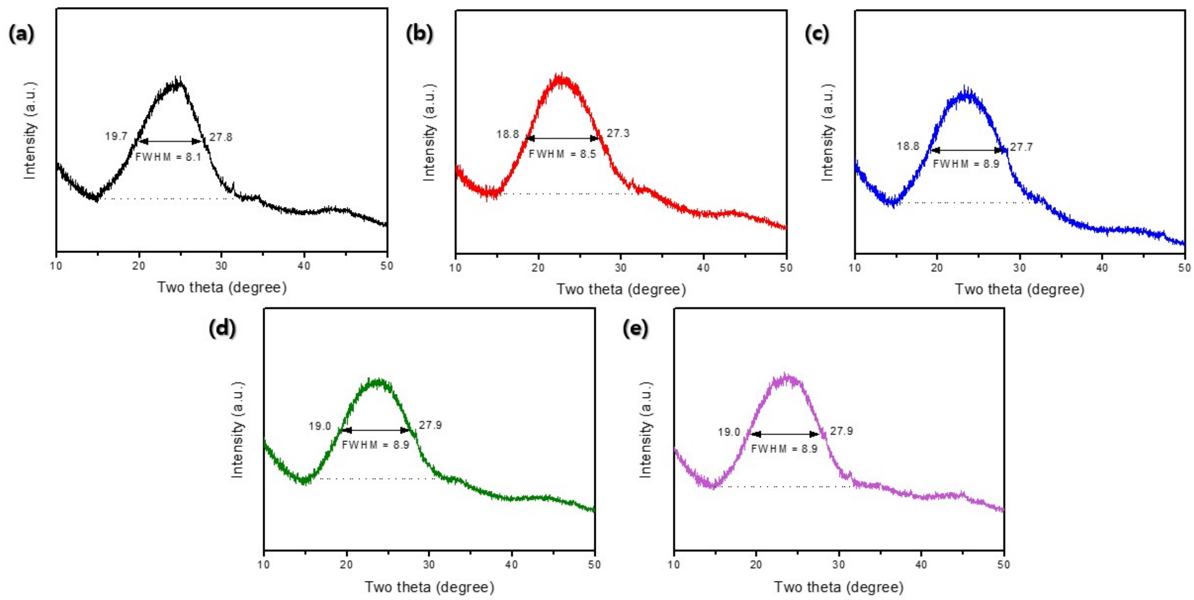

Fig. S11. XRD patterns at low angle and FWHM values of (a) c-PAN, (b) c-PAN@MCA$_{0.125}$, (c) c-PAN@MCA$_{0.25}$, (d) c-PAN@MCA$_{0.375}$, and (e) c-PAN@MCA$_{0.5}$.

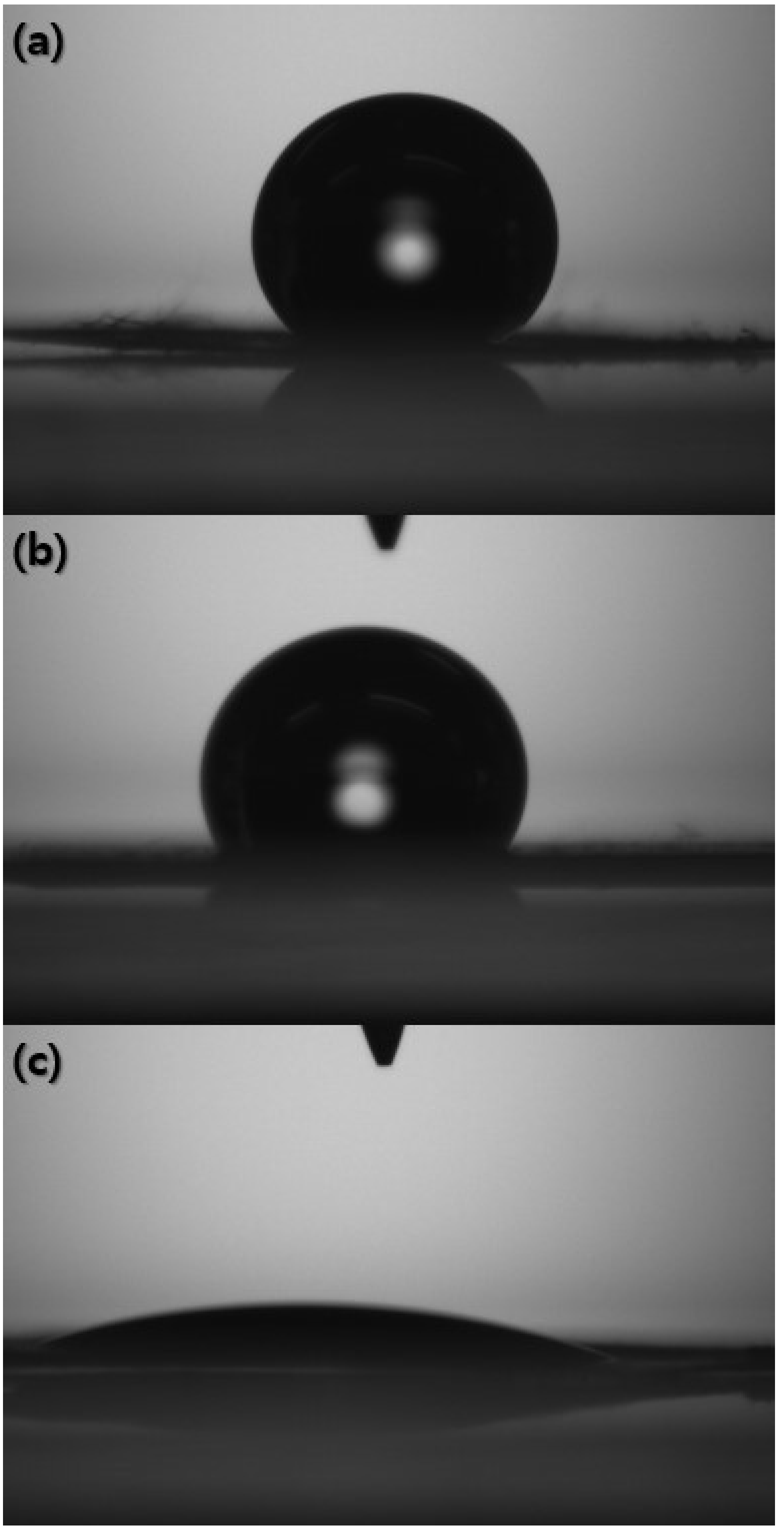

Fig. S12. Contact angle measurements for (a) c-PAN, (b) c-PAN@MCA$_{0.125}$, and (c) c-PAN@MCA$_{0.25}$.

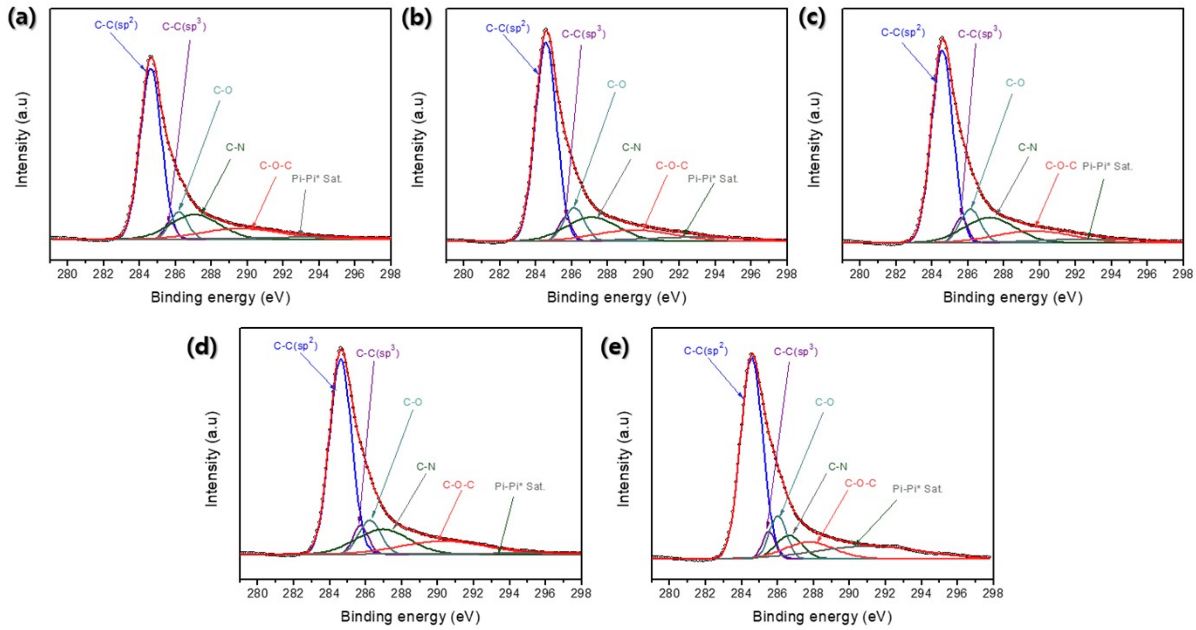

Fig. S13. Enlarged views of high-resolution XPS C1s spectra of (a) c-PAN, (b) c-PAN@MCA$_{0.125}$, (c) c-PAN@MCA$_{0.25}$, (d) c-PAN@MCA$_{0.375}$, and (e) c-PAN@MCA$_{0.5}$.

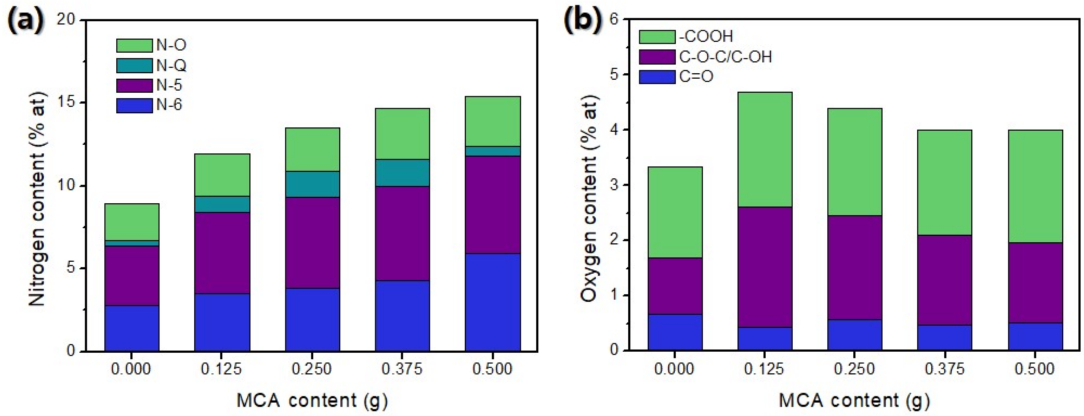

Fig. S14. (a) Nitrogen contents of c-PAN and c-PAN@MCA nanofibers from high-resolution XPS N1s spectra. (b) Oxygen contents of c-PAN and c-PAN@MCA nanofibers from high-resolution XPS O1s spectra.

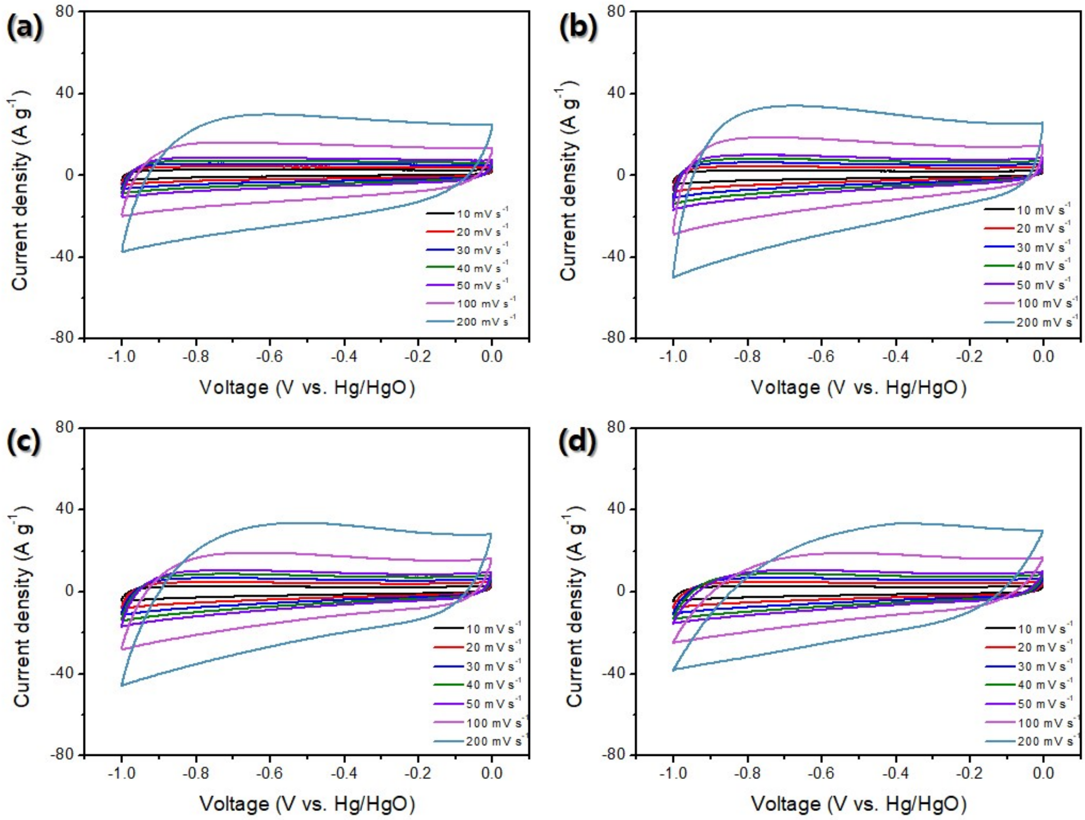

Fig. S15. CV curves of (a) c-PAN, (b) c-PAN@MCA$_{0.125}$, (c) c-PAN@MCA$_{0.375}$, and (d) c-PAN@MCA$_{0.5}$ at various scan rates.

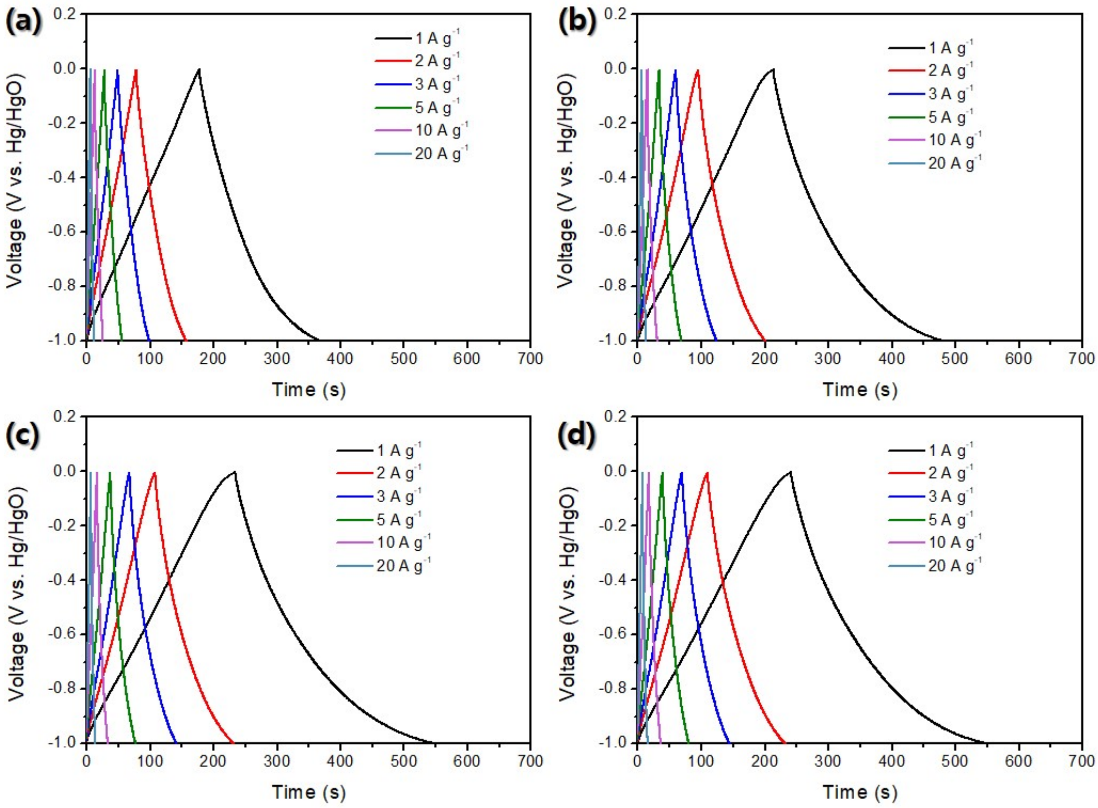

Fig. S16. GCD curves of (a) c-PAN, (b) c-PAN@MCA$_{0.125}$, (c) c-PAN@MCA$_{0.375}$, and (d) c-PAN@MCA$_{0.5}$ at various current densities.

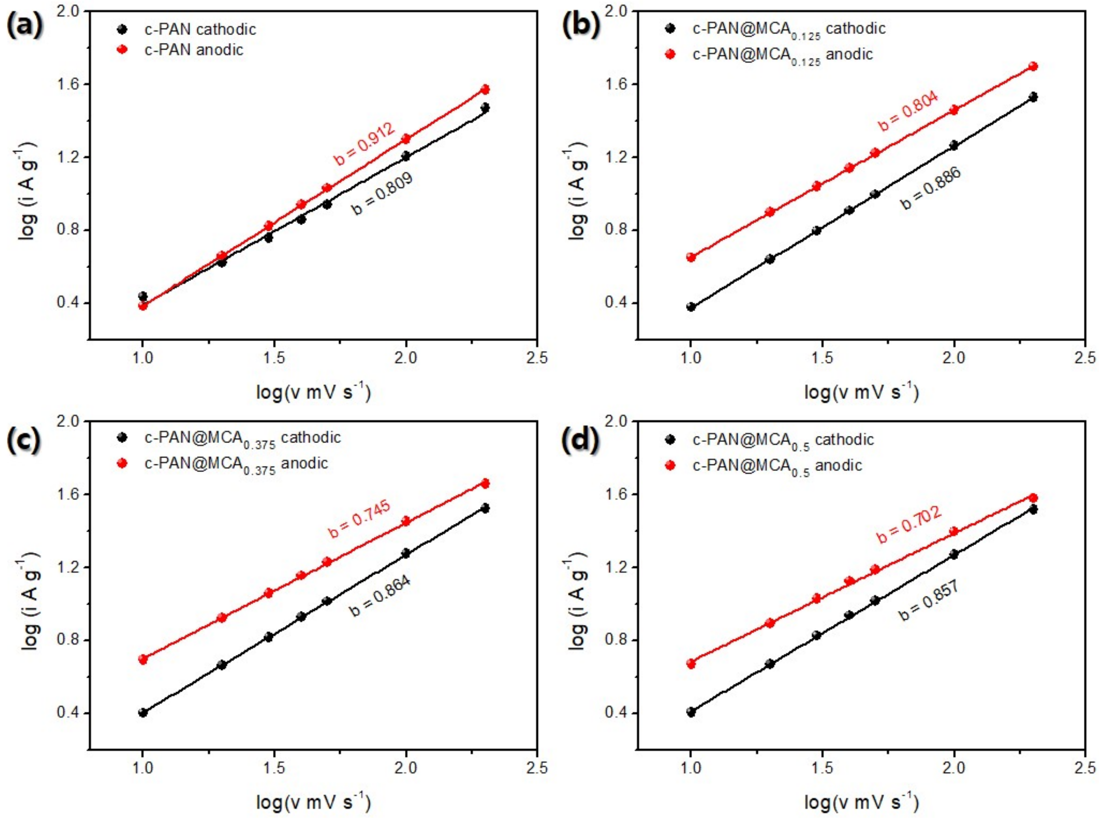

Fig. S17. Relationships between the peak current and scan rate for (a) c-PAN, (b) c-PAN@MCA$_{0.125}$, (c) c-PAN@MCA$_{0.375}$, and (d) c-PAN@MCA$_{0.5}$.

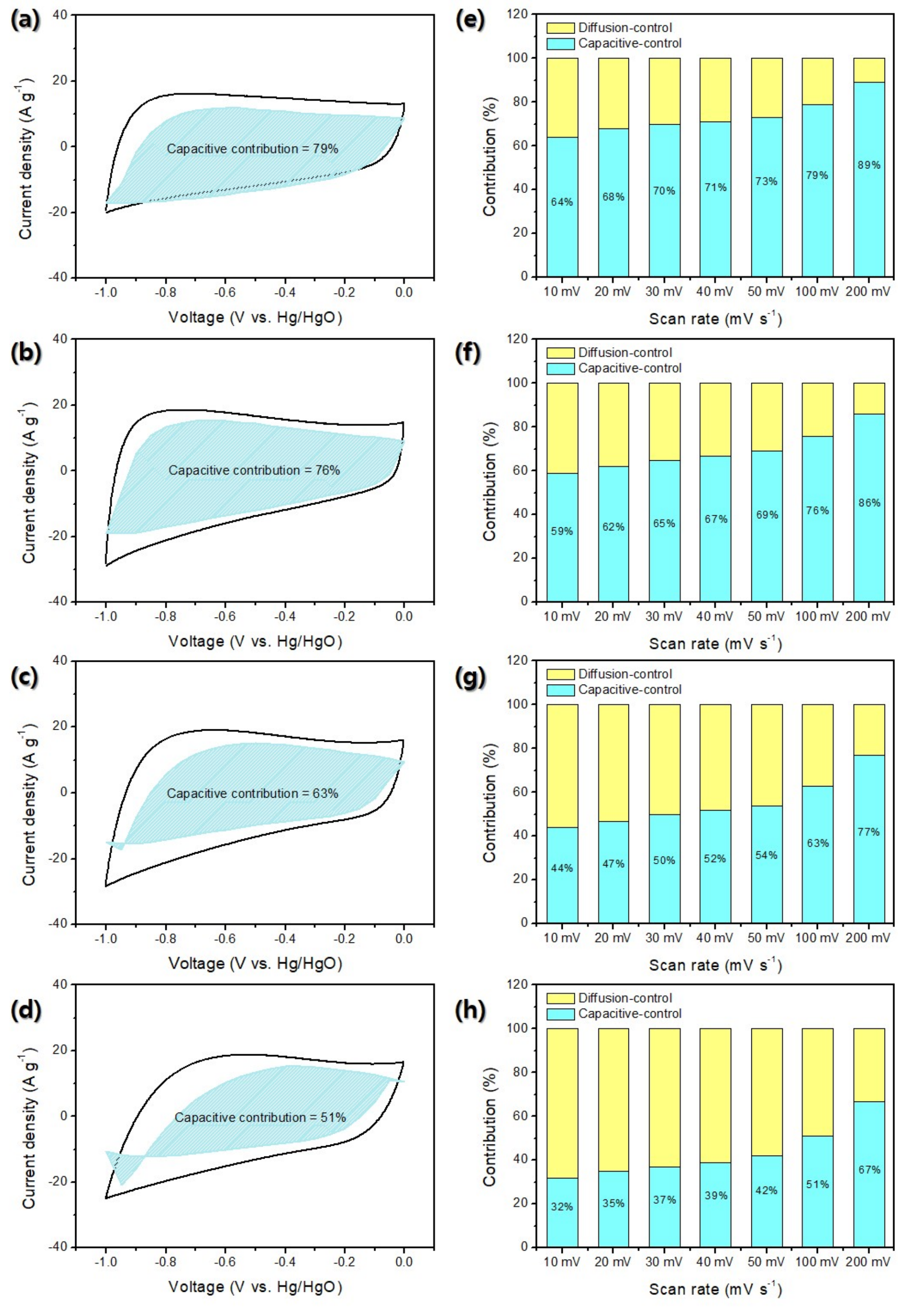

Fig. S18. Capacitive contributions at a scan rate of 100 mV s^{-1} for (a) c-PAN, (b) c-PAN@$MCA_{0.125}$, (c) c-PAN@$MCA_{0.375}$, and (d) c-PAN@$MCA_{0.5}$. (f) Capacitive contributions at various scan rates for (e) c-PAN, (f) c-PAN@$MCA_{0.125}$, (g) c-PAN@$MCA_{0.375}$, and (h) c-PAN@$MCA_{0.5}$.

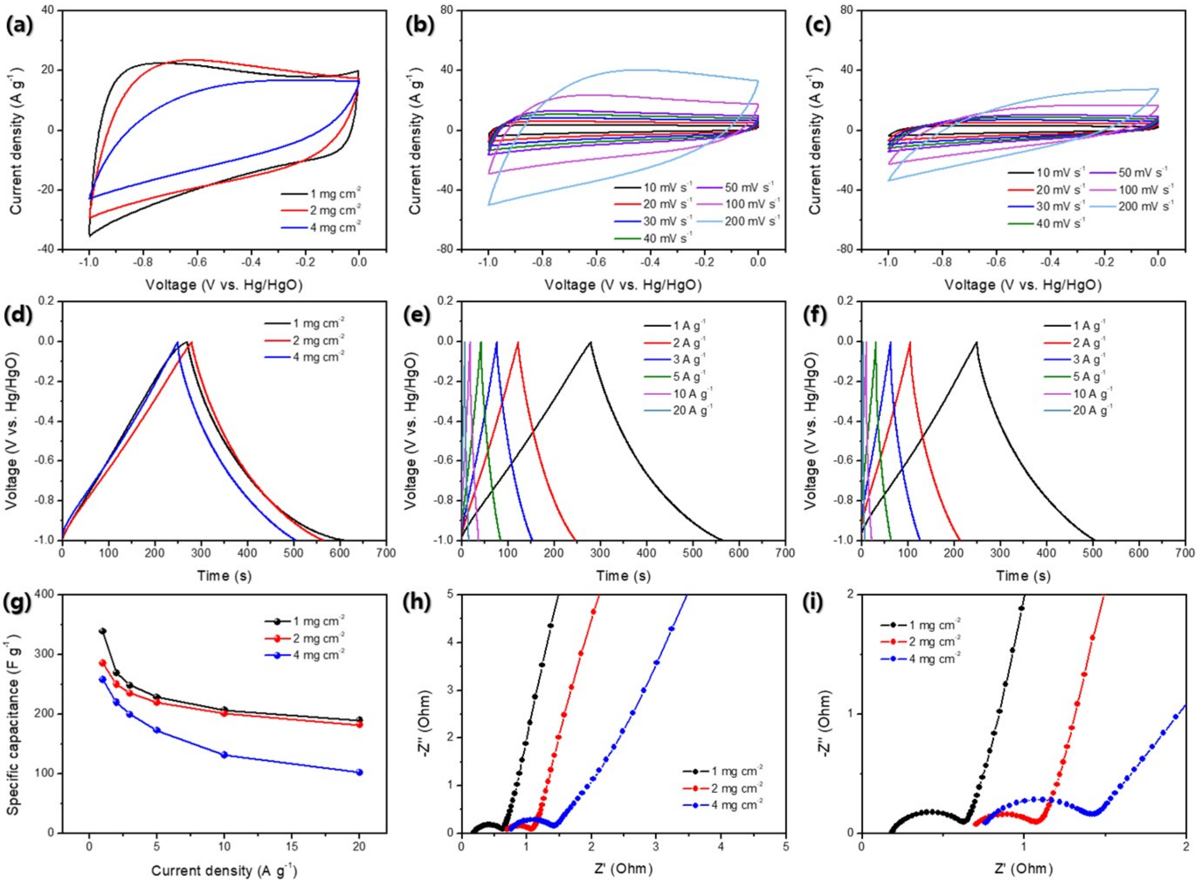

Fig. S19. Electrochemical performances of c-PAN@MCA$_{0.25}$ with different mass loadings measured in a three-electrode configuration in 6 M aqueous KOH electrolyte. (a) CV curves of c-PAN@MCA$_{0.25}$ with different mass loadings at a scan rate of 100 mV s^{-1}. CV curves of c-PAN@MCA$_{0.25}$ with mass loadings of (b) 2 mg cm^{-2} and (c) 4 mg cm^{-2} at various scan rates. (d) GCD curves of c-PAN@MCA$_{0.25}$ with different mass loadings at a current density of 1 A g^{-1}. GCD curves of c-PAN@MCA$_{0.25}$ with mass loadings of (e) 2 mg cm^{-2} and (f) 4 mg cm^{-2} at various current densities. (g) Specific capacitances at various current densities for c-PAN@MCA$_{0.25}$ with different mass loadings. (h, i) Nyquist plots of c-PAN@MCA$_{0.25}$ with different mass loadings.

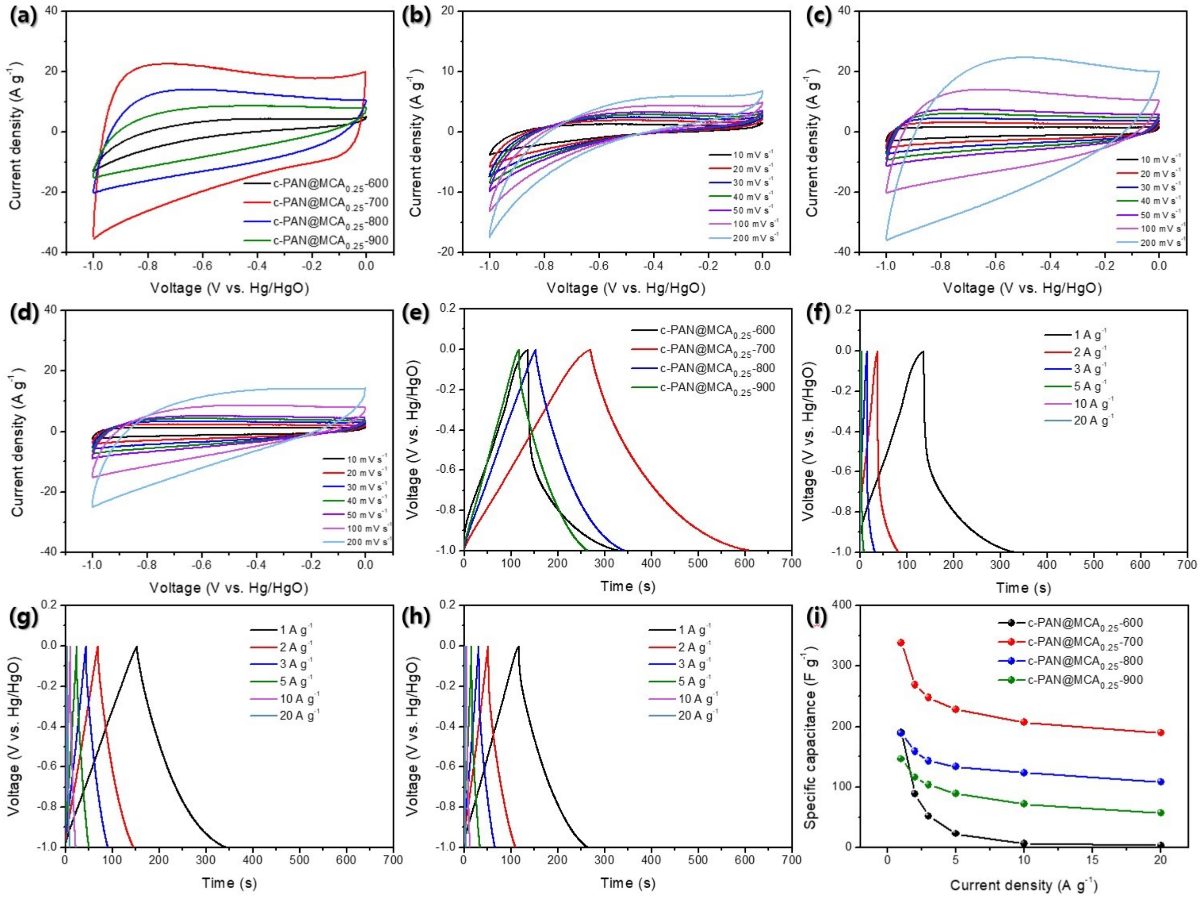

Fig. S20. Electrochemical performances of c-PAN@$MCA_{0.25}$ with different annealing temperatures measured in a three-electrode configuration in 6 M aqueous KOH electrolyte. (a) CV curves of c-PAN@$MCA_{0.25}$ with different annealing temperatures at a scan rate of 100 mV s^{-1}. CV curves of c-PAN@$MCA_{0.25}$ with annealing temperatures of (b) 600, (c) 800, and (d) 900 °C at various scan rates. (e) GCD curves of c-PAN@$MCA_{0.25}$ with different annealing temperatures at a current density of 1 A g^{-1}. GCD curves of c-PAN@$MCA_{0.25}$ with mass loadings of (f) 600, (g) 800, and (h) 900 °C at various current densities. (i) Specific capacitances at various current densities for c-PAN@$MCA_{0.25}$ with different annealing temperatures.

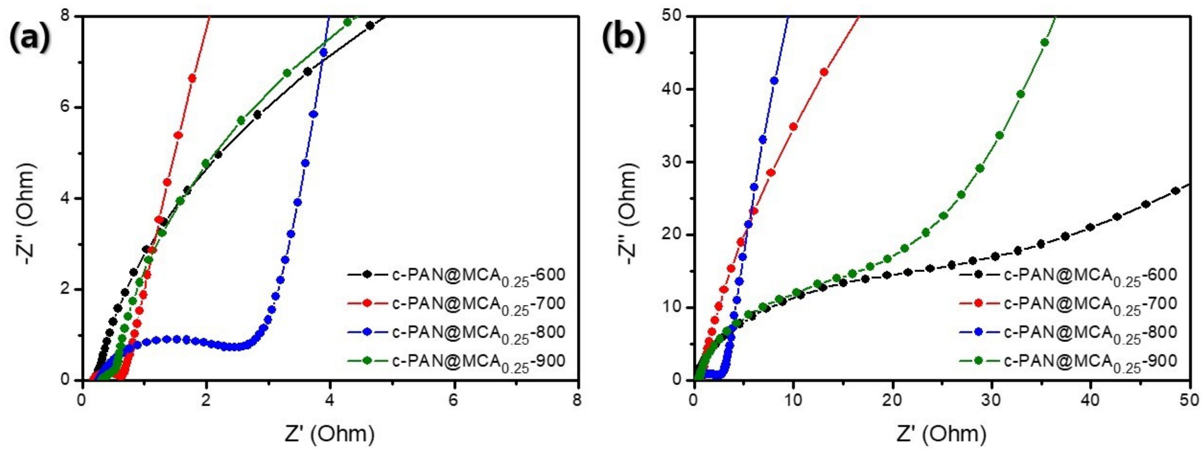

Fig. S21. (a, b) Nyquist plots of c-PAN@MCA$_{0.25}$ with different annealing temperatures.

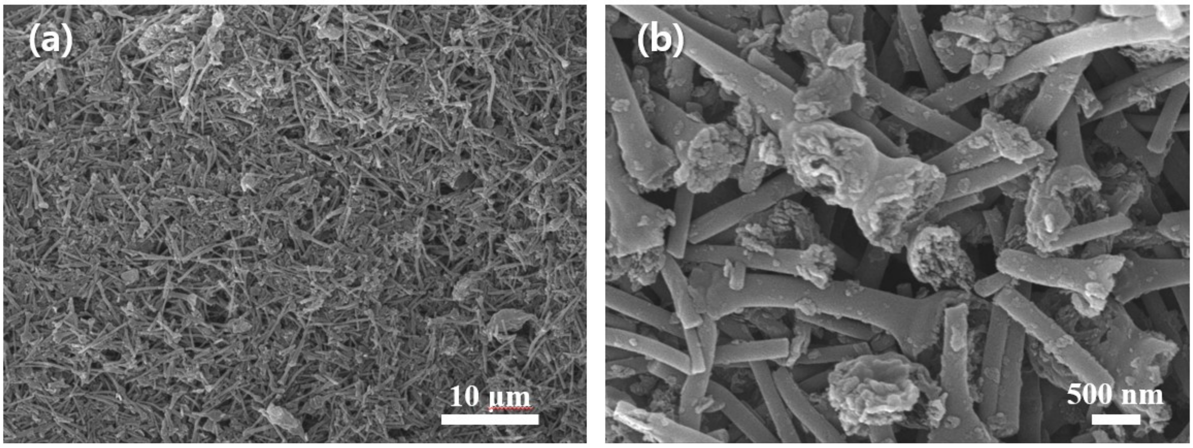

Fig. S22. (c, b) SEM images of ground c-PAN@$MCA_{0.25}$ nanofiber.

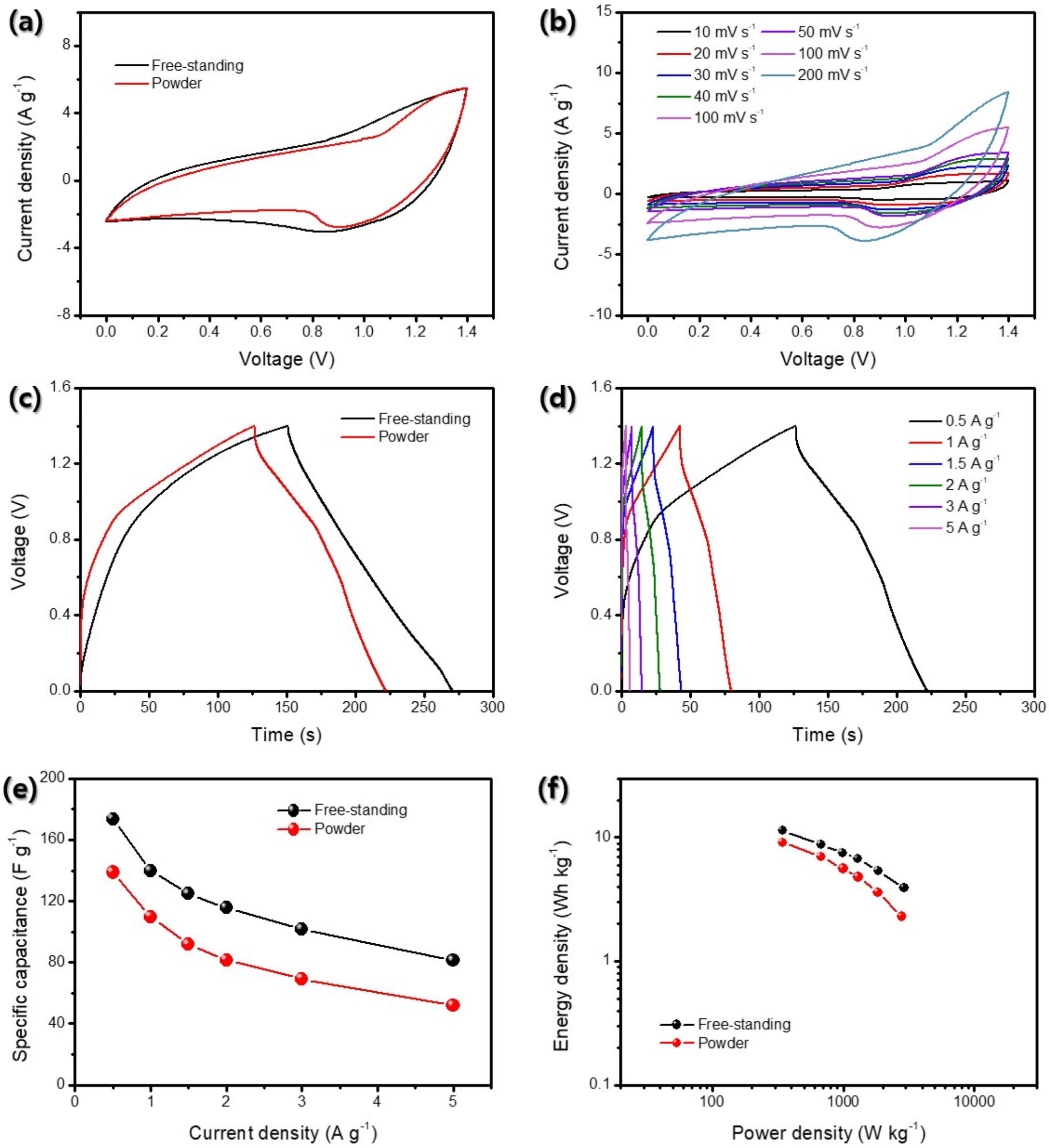

Fig. S23. Electrochemical performance measured in a two-electrode configuration in 1 M aqueous Na_2SO_4 electrolyte. (a) CV curves for free-standing and ground c-PAN@MCA$_{0.25}$-based symmetric SC at a scan rate of 100 mV s^{-1}, respectively. (b) CV curves of ground c-PAN@MCA$_{0.25}$-based symmetric SC at various scan rates. (c) GCD curves for free-standing and ground c-PAN@MCA$_{0.25}$-based symmetric SC at a current density of 1 A g^{-1}, respectively. (d) GCD curves of ground c-PAN@MCA$_{0.25}$-based symmetric SC at various current densities. (e) Specific capacitances of free-standing and ground c-PAN@MCA$_{0.25}$-based symmetric SC at various current densities, respectively. (f) Ragone plot for free-standing and ground c-PAN@MCA$_{0.25}$-based symmetric SCs, respectively.

To measure the electrochemical performance of powder-type c-PAN@MCA$_{0.25}$, ground c-PAN@MCA$_{0.25}$ was mixed uniformly with carbon black, and poly(vinylidene fluoride) with a mass ratio of 8:1:1 and then pasted onto the nickel foam (1 x 2 cm^2). The active mass in each electrode was fixed at 1 mg cm^{-2}.

Table S1. BET surface area (S_{BET}), total pore volume (V_{total}), micropore volume (V_{micro}) and mesopore volume (V_{meso}) of c-PAN and c-PAN@MCA nanofibers.

	S_{BET} (m^2 g^{-1})	V_{total} (cm^3 g^{-1})	V_{micro} (cm^3 g^{-1})	V_{meso} (cm^3 g^{-1})
c-PAN	7.1	0.027	0.026	0.001
c-PAN@MCA$_{0.125}$	335.1	0.211	0.084	0.127
c-PAN@MCA$_{0.25}$	403.1	0.358	0.212	0.146
c-PAN@MCA$_{0.375}$	368.5	0.321	0.187	0.134
c-PAN@MCA$_{0.5}$	347.6	0.463	0.346	0.117

Table S2. Atomic concentrations for c-PAN and c-PAN@MCA nanofibers.

	C (at%)	N (at%)	O (at%)
c-PAN	87.8	8.8	3.4
c-PAN@MCA$_{0.125}$	83.4	11.9	4.7
c-PAN@MCA$_{0.25}$	82.1	13.5	4.4
c-PAN@MCA$_{0.375}$	81.3	14.7	4.0
c-PAN@MCA$_{0.5}$	80.6	15.4	4.0

Table S3. Summary of the electrochemical performance of c-PAN@MCA$_{0.25}$ and the state-of-the-art carbon nanofiber electrodes.

Electrode sample name	Specific capacitance (three-electrode configuration)	Energy density	Power density	Mass loading	Reference
c-PAN@MCA$_{0.25}$	338.6 F g^{-1} (1 A g^{-1})	11.4 Wh kg^{-1}	344 W kg^{-1}	1 mg cm^{-2}	This work
	285.7 F g^{-1} (1 A g^{-1})	N/A	N/A	2 mg cm^{-2}	
	257.8 F g^{-1} (1 A g^{-1})	N/A	N/A	4 mg cm^{-2}	
CLCF	223.8 F g^{-1} (0.5 A g^{-1})	5.9 Wh kg^{-1}	1200 W kg^{-1}	1.2 mg cm^{-2}	1
MCF	105 F g^{-1} (5 mV s^{-1}, two-electrode configuration)	5.1 Wh kg^{-1}	242 W kg^{-1}	0.44 mg cm^{-2}	2
P-CNF	104 F g^{-1} (0.2 A g^{-1})	3.22 Wh kg^{-1}	600 W kg^{-1}	0.51 mg cm^{-2}	3
PHCNF30	239 F g^{-1} (1 A g^{-1})	5.28 Wh kg^{-1}	500 W kg^{-1}	2 mg cm^{-2}	4
C67$_{14}$@PAN-OC	270 F g^{-1} (1 A g^{-1})	9.64 Wh kg^{-1}	550 W kg^{-1}	N/A	5
NHCF	302 F g^{-1} (0.5 A g^{-1})	N/A	N/A	1 mg cm^{-2}	6
UT-CNF	243 F g^{-1} (1 A g^{-1})	N/A	N/A	1.2-1.4 mg cm^{-2}	7
CACNF	202 F g^{-1} (0.1 A g^{-1})	N/A	N/A	1.5 mg cm^{-2}	8
NFMCNF	252.6 F g^{-1} (0.5 A g^{-1})	8.07 Wh kg^{-1}	248 W kg^{-1}	N/A	9
N-CNT@CF	367 F g^{-1} (0.5 A g^{-1})	5.5 Wh kg^{-1}	254 W kg^{-1}	1.0-1.2 mg cm^{-2}	10
NC-800	264 F g^{-1} (1 A g^{-1})	N/A	N/A	1.5 mg cm^{-2}	11
N-PCNFA	279 F g^{-1} (0.5 A g^{-1})	N/A	N/A	N/A	12
PAN/NOC (7:3)	394 F g^{-1} (1 A g^{-1})	13.6 Wh kg^{-1}	500 W kg^{-1}	1.67 mg cm^{-2} (powder)	13
HPCNFs-N	307.2 F g^{-1} (1 A g^{-1})	10.96 Wh kg^{-1}	250 W kg^{-1}	1.0 mg cm^{-2} (powder)	14
NSCPCNF-800	396 F g^{-1} (1 A g^{-1})	14.3 Wh kg^{-1}	250 W kg^{-1}	1.0 mg cm^{-2}	15

References

1. Y. Cheng, L. Huang, X. Xiao, B. Yao, L. Yuan, T. Li, Z. Hu, B. Wang, J. Wan and J. Zhou, *Nano Energy*, 2015, **15**, 66-74.

2. Z. Liu, D. Fu, F. Liu, G. Han, C. Liu, Y. Chang, Y. Xiao, M. Li and S. Li, *Carbon*, 2014, **70**, 295-307.

3. Y. Liu, J. Zhou, L. Chen, P. Zhang, W. Fu, H. Zhao, Y. Ma, X. Pan, Z. Zhang, W. Han and E. Xie, *ACS Apple. Mater. Interfaces*, 2015, **7**, 23515-23520.

4. J.-G Kim, H.-C. Kim, N. D. Kim and M.-S Khil, *Compos. B Eng.*, 2020, **186**, 107825.

5. C.-H Yang, Y.-C. Hsiao and L.-Y Lin, *ACS Appl. Mater. Interfaces*, 2021, **13**, 41637-41648.

6. Y. Yao, H. Wu, L. Huang, X. Li, L. Yu, S. Zeng, X. Zeng, J. Yang and J. Zou, *Electrochim. Acta*, 2017, **246**, 606-614.

7. W. M. Chang, C. C. Wang and C. Y. Chen, *Electrochim. Acta*, 2019, **296**, 268-275.

8. Q. Fan, C. Ma, L. Wu, C. Wei, H. Wang, Y. Song and J. Shi, *RSC Adv.*, 2019, **9**, 6419-6428.

9. W. Na, J. Jun, J. W. Park, G. Lee and J. Jang, *J. Mater. Chem. A*, 2017, **5**, 17379-17387.

10. T. P. Mofokeng, Z. N. Tetana and K. I. Ozoemena, *Carbon*, 2020, **169**, 312-326.

11. Q. Jiang, M. Liu, C. Shao, X. Li, H. Liu, X. Li and Y. Liu, *Electrochim. Acta*, 2020, **330**, 135212.

12. Y. Yang, Y.-x. Liu, Y Li, B.-w. Deng, B. Yin and M.-b Yang, *J. Mater. Chem. A*, 2020, **8**, 17257.

13. H. Wang, H. Niu, H. Wang, W. Wang, X. Jin, H. Wang, H. Zhou and T. Lin, *J. Power Sources*, 2021, **482**, 228986.

14. L-F Chen, Y. Lu, L. Yu and X. W. Lou, *Energy Environ. Sci.*, 2017, **10**, 1777-1783.

15. Y. Li, G. Zhu, H. Huang, M. Xu, T. Lu and L. Pan, *J. Mater. Chem. A*, 2019, **7**, 9040-9050

Supplementary movie 1_c-PAN@M

Supplementary movie 2_c-PAN@M